

*Letter to the Editor***Observation of oscillations in coronal loops****I. De Moortel¹, J. Ireland², and R.W. Walsh¹**¹ University of St Andrews, School of Mathematical and Computational Sciences, North Haugh, St Andrews, Fife KY16 9SS, Scotland² ESA at NASA Goddard Spaceflight Center, Room G-1, Building 26, Mail Code 682.3, Greenbelt, Maryland 20771, USA

Received 15 December 1999 / Accepted 28 January 2000

Abstract. On March 23rd 1999, a set of TRACE observations in the 171 Å (Fe IX) bandpass was made of active region AR 8496. A wavelet analysis of a bright loop-footpoint to the south west of this active region displays outward propagating perturbations with periods 180–420 seconds at approximately 70–165 km s⁻¹. We suggest that these oscillations are slow magneto-acoustic waves propagating along the loop, carrying an estimated energy flux of 4×10^2 ergs cm⁻² s⁻¹.

Key words: Magnetohydrodynamics (MHD) – Sun: activity – Sun: corona – Sun: oscillations

1. Introduction

Despite the widespread occurrence of hot coronae in the Sun and other stars, the coronal heating mechanism is still not fully understood. Over the past decades, several mechanisms have been suggested (Narain & Ulmschneider 1996; Browning 1991; Zirker 1993). The study of coronal oscillations is important since these oscillations could be associated with dissipating wave motions that could be heating of the solar corona. Obviously, the detection of such oscillations in the corona is a crucial step in determining the presence and relevance of these wave heating mechanisms.

DeForest & Gurman (1998) report on quasi-periodic compressive waves in solar polar plumes which Ofman et al. (1999) consider to be slow magneto-acoustic waves. More recently, Aschwanden et al. (1999) reported the first detection of spatial displacement oscillations of coronal loops, observed for the first time due to the high spatial resolution of the *Transition Region and Coronal Explorer* (TRACE) telescope. Nakariakov et al. (1999) analysed the transverse loop oscillations induced by a flare observed with TRACE in the 171 Å and 195 Å bandpass and estimated the damping time. From the damping time Nakariakov et al. (1999), estimated that the coronal dissipation coefficient could be as much as eight or nine orders of magnitude larger than the theoretically predicted classical value. This larger dissipation coefficient may solve some of the existing difficulties with wave heating and reconnection theories.

Send offprint requests to: ineke@mcs.st-and.ac.uk

In this paper we report on the detection of propagating oscillations out from the footpoints of a large diffuse coronal loop structure close to an active region as observed in 171 Å by TRACE. A first report on small scale EUV brightenings in the same high cadence (9 s) TRACE data was given by Ireland et al. (1999b). As in Ireland et al. (1999a, b), we employ a wavelet analysis to investigate significant periodicity in the observed oscillations.

The observations and preparation of the data are described in Sect. 2. Sect. 3 presents the method and the results of the data analysis. An interpretation in terms of physical wave modes is given in Sect. 4. Sect. 5 provides a brief summary.

2. Observations

The analysis in this paper is based upon TRACE 171 Å (Fe IX) observations of active region AR 8496; a large, stable active region present in the southwest quadrant on 23 March 1999. The data are taken as part of Joint Observing Programme 83 - *High cadence activity studies and the heating of coronal loops*. The aim of this study was to reduce the cadence of the TRACE observations as low as possible while still retaining enough counts that events of interest would not be lost in the noise. The sequence, start time 0647 UT, consisted of 157 512×512 pixel images in the TRACE 171 Å bandpass with a 9 s cadence and with a pixel size of 1". The data is prepared in the same way as in Ireland et al. (1999b). As the data covers only a relatively short period, it has not been corrected for solar rotation. Fig. 1 shows an image of AR 8496. This is the first of the 0647 UT sequence on which we will be concentrating in this paper. The tube-like area that is indicated in the inset in Fig. 1 shows the region we will be looking at in detail. From this figure we see that the bright footpoint is about 40 arcsec long.

3. Analysis and results

To obtain results above a satisfactory confidence level, it is necessary to sacrifice some of the spatial and temporal resolution of this dataset. The original datacube consisted of 157 images with a 9 second cadence. To increase the signal-to-noise ratio, a datacube with 78 images with a 18 second cadence was

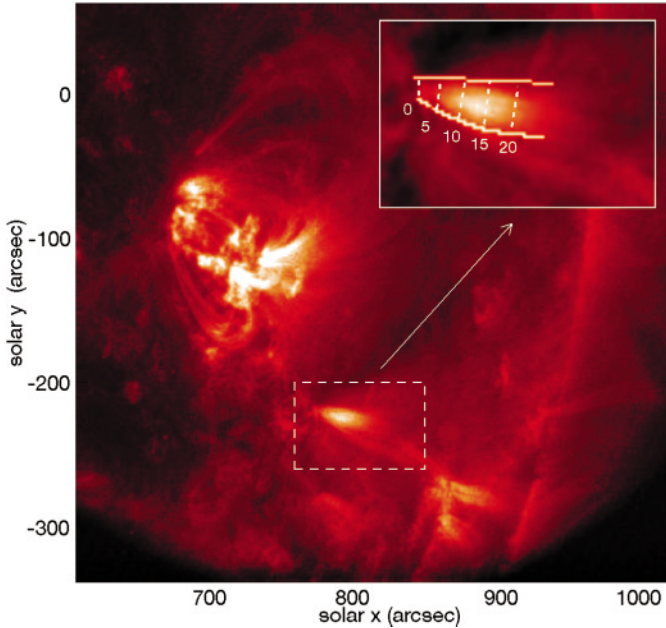


Fig. 1. Typical image in the 0647 UT 171 Å dataset. Inset is a blow up of the area supporting the oscillatory signal.

created by summing over consecutive images. To analyse the evolution of the region's brightness, we divide the region into 50 cross-sections. Both arcs that form the tube are normalised and cross-sections are then defined by connecting corresponding positions as is shown in the inset in Fig. 1. To emphasise the time-variable aspect of the behaviour of the region, we create a running-difference image of the average time series for each position. From each frame we subtracted the frame taken 90 seconds earlier. In order to obtain a uniform normalisation, we added all the unique datacounts along two consecutive cross-sections and divided by the number of counts. This is then defined to be the *average* timeseries for each of the 25 positions along the tube. Note that the datacube now has half of the time and spatial resolution of the original.

In the running-difference image (Fig. 2), some bright and dark features can be seen clearly running across the image with positive gradients. These diagonal ridges represent outward travelling regions of slightly higher (bright) or lower (dark) intensity. This indicates that a disturbance is travelling along the structure. The propagation speed of these features can be calculated by measuring their slope in the running-difference image. This speed has been calculated to be $\sim 70 - 16 \text{ km s}^{-1}$ throughout the time sequence. Taking into account line-of-sight projections, this range gives us a lower limit for the propagation speed of the disturbances. There is no significant deceleration or acceleration of the features as they propagate as the gradients in the running-difference are relatively constant. These oscillations are real time variations in intensity since motions of bright features due to solar rotation would result in much slower variations. For the first half of the region, the amplitude of the disturbance is a variation of 2%-4% compared to the background brightness, which is more than twice the amplitude of

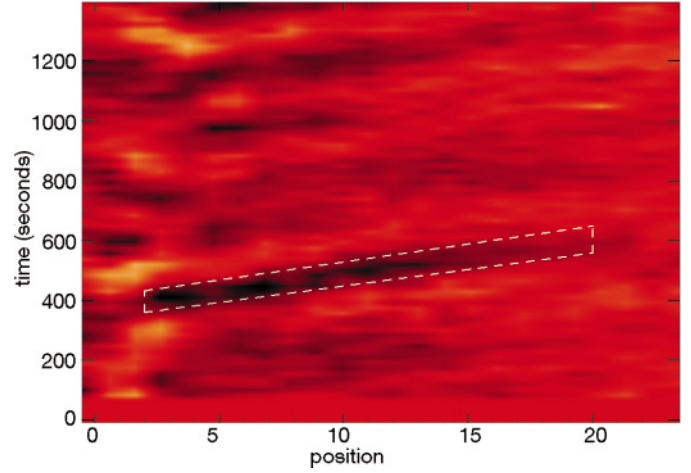


Fig. 2. A plot of the running difference between the average time series for each position along the inner arc

the expected noise level. The signal gets weaker as it propagates along the structure; there is about a 0.6%-2% variation in the background brightness which is only just above the noise level when the signal reaches the end of the analysed region. So there appears to be evidence that the amplitude of the disturbances decreases as they travel along the structure.

3.1. Wavelet analysis

To determine an oscillation timescale in the data, we introduce a wavelet analysis at different positions along the tube. Methods such as the Fast Fourier Transform calculate power at particular frequencies by analysing the entire time series. The Fourier transform provides information about the frequency domain but all time localised information is lost in this process. However, wavelet analysis is an important extension of Fourier analysis as it provides the time localisation of the frequency components. This makes the wavelet analysis ideal for analysing time series where one expects localised variations of power. We will give a brief overview of the method but for further details we refer the reader to Torrence and Compo (1998). We follow the analysis described by Ireland et al. (1999a, b).

Let us assume we have a time series x_n of N observations with sample interval δt . The continuous wavelet transform is then defined as the convolution of x_n with an analysis (or mother) wavelet $\psi(\eta)$. We assume that ψ is normalised, i.e. $\int_{-\infty}^{\infty} \psi \psi^* d\eta = 1$. For $\eta = (n' - n)\delta t/s$ we have

$$W_n(s) = \sum_{n'=0}^{N-1} x_{n'} \sqrt{\frac{\delta t}{s}} \psi^* \left[\frac{(n' - n)\delta t}{s} \right], \quad (1)$$

where s is the wavelet scale and n allows us to translate the analysing wavelet in time. By varying s and n , one can build up a picture of any features in the time series as a function of the scale s and the localised time index n .

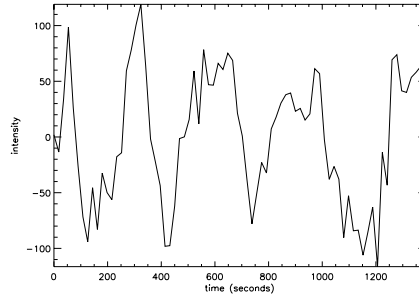
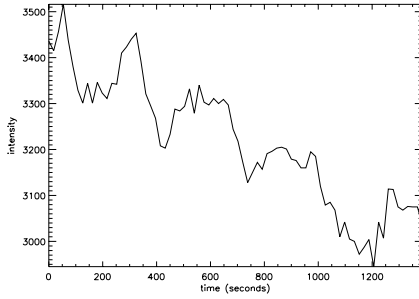


Fig. 3. An overview of the raw (left) and processed (right) intensity variations at position 4 along the region shown in Fig. 1

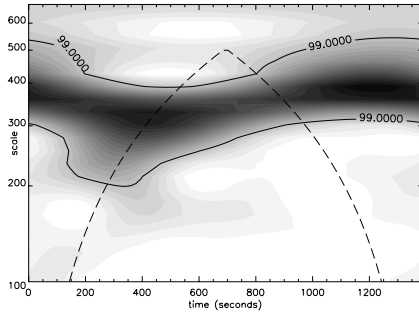


Fig. 4. Wavelet analysis at position 4 along the tube (confidence level=99.0%). Darker colours correspond to higher wavelet power. The dashed line indicates the cone of influence.

To analyse our oscillatory signal, we will use the Morlet wavelet,

$$\psi(\eta) = \pi^{-1/4} \exp(6i\eta) \exp\left(-\frac{\eta^2}{2}\right), \quad (2)$$

consisting of a plane wave modulated by a Gaussian, as our mother wavelet. The wavelet power spectrum is defined as $|W_n(s)|^2$. Ranging through s and n will build up a two-dimensional time-frequency transform of the original time series. The wavelet transform also suffers from edge effects at both ends of the time series. This results in a *cone of influence* in the transform, indicated as a dashed line in Fig. 4. Portions of the transform outside the area formed by the time axis and the cone of influence are subject to these edge effects. To put a confidence level in the analysis, we assume that the noise in our TRACE data is Poissonian, that is, if x DN are observed then the Poisson noise in such measurement is $\sigma_{\text{noise}}(x) = \sqrt{x}$. We chose a 99.0% confidence level in our analysis above which we consider any wavelet power as real. Therefore, there is a 1.0% chance that the observed wavelet power is due to chance. The same running difference and wavelet method was applied to Quiet Sun regions in the same dataset but no significant periodicity was found.

The left plot of Fig. 3 shows the original data at position 4 along the tube like region as defined in Fig. 1. The right plot shows the “processed” data at this position; that is, a linear polynomial is fitted to the original data and subtracted subsequently from the original data. Just from a visual inspection, we already see that at this position, there is a signal with a period of roughly 300 seconds for the entire duration of the observation. The results from the wavelet analysis for position 4 are shown

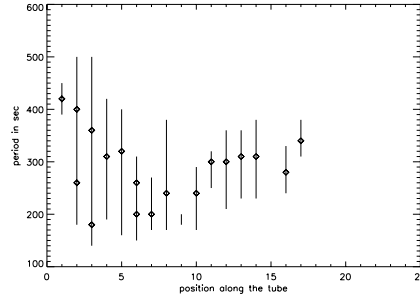


Fig. 5. An overview of the results (0647 UT, 171 Å) for all positions along the tube (confidence level=99.0%)

in Fig. 4. A clear band of strong wavelet power, situated between 250 and 350 seconds, above the 99.0% confidence level, is detected running throughout the entire time interval.

This analysis was repeated for all the positions along the tube and an overview of the results is given in Fig. 5. This figure shows the range of periods that are picked up for each position, above the 99.0% confidence level. From this we see that the periods are situated between 140 s and 500 s. The diamonds in Fig. 5 indicate where the strongest wavelet power is situated for each position, which ranges from 180 s to 420 s.

A second observational sequence, starting at 0822 UT, consisted of 78 512×512 pixel images in both the TRACE 171 and 195 Å bandpass with an 18 s cadence and same pixel size. For the second 171 Å dataset of the same region, the running-difference image shows similar bright and dark diagonal bands, with similar properties but they seemed to be confined to the lower half of the region. In the 195 Å dataset, the region we are looking at is much fainter but similar diagonal features still appear in the running-difference image.

4. Discussion

In the magnetically dominated corona, structures are expected to undergo three types of oscillations, driven by different restoring forces: non-compressional Alfvén waves, where the restoring force is provided by the magnetic tension, and slow and fast magneto-acoustic waves, where the magnetic and kinetic pressures are the restoring forces (Porter et al. 1994a, 1994b; Roberts et al. 1984). While Alfvénic oscillations are essentially velocity oscillations and do not cause any variation in the intensity, the compressional waves cause density changes. Therefore, they could be observed in the form of intensity variations, pro-

vided there are no associated temperature changes big enough to bring the material outside the 171 Å bandpass.

Since the data displays propagating variations in the intensity (Fig. 2), these could be interpreted as magneto-acoustic modes. The moving features that are visible in the loop footpoint region travel at a constant speed throughout our field of view, i.e. there appears to be no significant deceleration or acceleration. As they are travelling at the order of the coronal sound speed ($c_s \sim 150 \text{ km s}^{-1}$), we consider these propagating oscillations to be good candidates for being propagating slow magneto-acoustic waves, similar to the propagating features found in polar plumes by DeForest et al. (1998). Ofman et al. (1999) calculated the acoustic cutoff frequency to be $\omega_{\text{cutoff}} \approx 1.5 \times 10^{-3} \text{ rad s}^{-1}$ and consequently, waves with periods over 70 minutes would be evanescent. As the oscillations we observed have much shorter periods, the waves are travelling into the corona. Following Ofman et al. (1999), we can estimate the energy flux carried the slow magneto-acoustic waves as $\rho[(\delta v)^2/2]v_s$, where δv is the wave velocity amplitude and $v_s \approx c_s = 150 \text{ km s}^{-1}$ in the corona. Using $\rho = 5 \times 10^{-16} \text{ g cm}^{-3}$ and $\delta v = 3 \text{ km s}^{-1}$, we get an upper bound for the wave energy flux $\sim 3.5 \times 10^2 \text{ ergs cm}^{-2} \text{ s}^{-1}$. This energy is only a very small fraction of the total energy required to heat coronal loops. The above interpretation is only valid if we assume the loop to be linear and homogeneous. For a non-linear, non-homogeneous medium, there could be several other possible interpretations such as nonlinear waves and mode coupling. Signatures of compressional waves in polar plumes were first detected by the White Light Channel of the UVCS instrument on SOHO high above the limb by Ofman et al. (1997). Unlike the observations done by Aschwanden et al. (1999), no flare occurred during or just before our observations.

5. Conclusions

We have analysed intensity variations of an active region coronal loop, observed by TRACE in the 171 Å bandpass. We interpreted these oscillations as propagating slow magneto-acoustic waves, carrying an estimated energy flux of $4 \times 10^2 \text{ ergs cm}^{-2} \text{ s}^{-1}$. We found periods with the strongest power in the 180-420 s range and velocities of the order of 70 - 165 km s^{-1} .

Due to the coincidence with the photospheric 5-minute period, there could be some form of coupling between the photosphere and the coronal loop, e.g. in the form of photospheric driving of the loop footpoints. The observation of coronal oscillations has important consequences as it could provide us with useful information for many numerical or analytical models of wave heating in the solar corona. Other possible interpretations of the propagating disturbances and the damping of their amplitude as they travel along the structure, will be addressed in De Moortel et al. (2000). Further details of the 0822 UT datasets and of the active region AR 8496 itself will also be discussed.

Acknowledgements. The authors would like to thank L. Ofman, A.W. Hood and D.S. Brown for useful comments and critical reading of the manuscript. Wavelet software was provided by C. Torrence and G. Compo, and is available at URL: <http://paos.colorado.edu/research/wavelets>. I. De Moortel is supported by E.U. grant ERBFMBICT982880.

References

- Aschwanden, M.J., Fletcher, L., Schrijver, C.J., Alexander, D., 1999, *ApJ* 520, 880
- Browning, P.K., 1991, *Plasma Phys. and Controlled Fusion* 33, 539
- DeForest, C.E., Gurman, J.B., 1998, *ApJ* 501, L217
- De Moortel, I., Ireland, J., Walsh R.W., 2000, *in preparation*
- Ireland, J., Walsh, R.W., Harrison, R.A., Priest, E.R., 1999a, *ESA-SP* 446
- Ireland, J., Wills-Davey, M., Walsh, R.W., 1999b, *Solar Physics, in press*
- Nakariakov, V.M., Ofman, L., DeLuca, E.E., Roberts, B., Davila, J.M., 1999, *Science* 285, 862
- Narain, U., Ulmschneider, P., 1996, *SSR* 75, 453
- Ofman, L., Romoli, M., Poletto, G., Noci, C., Kohl, J.L., 1997, *ApJ* 491, L111
- Ofman, L., Nakariakov, V.M., DeForest, C.E., 1999, *ApJ* 514, 441
- Porter, L.J., Klimchuk, J.A., Sturrock, P.A., 1994a, *ApJ* 435, 482
- Porter, L.J., Klimchuk, J.A., Sturrock, P.A., 1994b, *ApJ* 435, 502
- Roberts, B., Edwin, P.M., Benz, A.O., 1984, *ApJ* 279, 857
- Torrence, C., Compo, G.P., 1998, *Bull. Amer. Meteor. Soc.* 79, 61
- Zirker, J.B., 1993, *Solar Physics* 148, 43